AIMS Mathematics, 6(10): 11005–11028.
DOI: 10.3934/math.2021639
Received: 10 May 2021
Accepted: 18 July 2021
Published: 30 July 2021

http://www.aimspress.com/journal/Math

Research article

Predefined-time vector-polynomial-based synchronization among a group of chaotic systems and its application in secure information transmission

Qiaoping Li[1,2,*] **and Sanyang Liu**[2]

[1] Zhengzhou University of Aeronautics, Zhengzhou 450015, China
[2] School of Mathematics and Statistics, Xidian University, Xi'an 710071, China

* **Correspondence:** Email: liqiaoping1981@126.com.

Abstract: This article aims to improve the security and timeliness of chaotic synchronization scheme in chaotic secure information transmission. Firstly, a novel nonlinear synchronization scheme among multiple chaotic systems is defined based on vector polynomial to improve the complexity of the carrier signal, and then to enhance the attack resistance of the communication scheme. Secondly, a more flexible and accurate synchronization control technology is proposed so that the above vector-polynomial-based chaotic synchronization can be realized within a time that is predefined as a tunable control parameter. Subsequently, the theoretical derivation is carried out to prove the synchronization time in the above-mentioned synchronization control scheme can be set independently without being affected by the initial conditions or other control parameters. Finally, several simulation experiments on secure information transmission are presented to verify the efficiency and superiority of the designed chaotic synchronization scheme and synchronization control technology.

Keywords: vector-polynomial-based synchronization; predefined-time control technique; fixed-time control technique; secure information transmission; image encryption
Mathematics Subject Classification: 93C10

1. Introduction

Along with the rapid development of mobile communication and Internet, as well as the rise of 5G network, the importance of information security is becoming more and more prominent. Due to its high nonlinearity, sensitivity to initial value and unpredictability of trajectory, chaotic system is especially suitable for constructing information encryption scheme with high security [1–5]. The realization of chaotic synchronization is the premise of the chaotic secure information transmission, therefore, it is of great significance to explore the chaotic synchronization scheme and synchronization control technique in depth [6–11].

For the chaotic secure communication, the level of security is mainly determined by the complexity level of the carrier signal which is generated by the drive system. However, the drive system in most chaotic secure communication schemes is a single chaotic system. If the drive system is composed of multiple systems, the carrier signal will become more complex and more unpredictable for decryption. Inspired by the above discussion, R. Luo presented a new type of synchronization scheme-combined synchronization, in which the drive system was a linear combination of two different chaotic systems with the same dimension [12]. However, since only linear operations of vector were used, the nonlinear characteristics of the combined drive system did not change essentially. Recently, Q. Li proposed the compound synchronization, in which the multiplication operation of matrix was first applied in the formation of the driving signal, so as to enhance the nonlinearity of the drive system [13]. However, the above-mentioned compound synchronization only considered the multiplication of two matrices. It is noted that the polynomial operation is a generalization of the multiplication operation. Therefore, if the polynomial operation can be used to formulate the drive system, the complexity of the carrier signal will be significantly improved. This inspires this work.

Notice the encrypted information will not be decoded until the synchronisation between the drive system and the response system is achieved. Fast synchronization is desired to prevent the loss of information during the initial phase of the secure communication. Therefore, finite-time chaotic synchronization emerged and a series of valuable research results have been obtained [14–20]. However, the synchronization time in finite-time chaotic synchronization has a strong dependence on the initial conditions. Recently, the concept called fixed-time chaotic synchronization has been developed to solve this problem, in which the synchronization time is uniformly bounded with respect to the initial conditions. Nevertheless, since the relationship between the control gains and the synchronization time is unclear, the synchronization time in fixed-time synchronization can not be accurately calculated [21–24]. With the continuous improvement of communication quality requirements, the designer would prefer to recover the encoded information within a predefined time according to the task requirements. Therefore, it is urgent to develop a novel concept of chaotic synchronization, in which the synchronization time can be predesigned off-line without being affected by the initial conditions or other system control gains [25–31]. This is anther goal for this work.

According to the above analysis, this article is dedicated to the design of a novel predefined-time vector-polynomial-based synchronization among multiple chaotic systems and its application in secure information transmission. The rest of this work is arranged as follows. In Section 2, a novel chaotic synchronization scheme is defined in virtue of the vector polynomial. After that, a novel concept named predefined-time vector-polynomial-based synchronization is proposed. In Section 3, a predefined-time synchronization control algorithm is designed to realize the above synchronization. In Section 4, a numerical simulation is presented to illustrate the validity of the above synchronization control algorithm. In Section 5, the proposed chaotic synchronisation scheme is applied in the information secure transmission to demonstrate its feasibility and superiority. Finally, Section 6 concludes this article.

The proposed approach includes two main contributions:

• Firstly, based on the concept of vector polynomial, the vector-polynomial-based synchronization scheme is presented, in which, the drive system is a compound chaotic system which is composed of several chaotic systems by linear operation and polynomial operation. Compared with other chaotic synchronization schemes, the compound drive system in this scheme has more complex

topology and less predictable chaotic path, which means that it has stronger anti-attack capability in secure information transmission. Moreover, the complexity of the compound drive system in this synchronization scheme can be changed by adjusting the coefficient or the degree of the vector polynomial.

• Secondly, the synchronization time can be set off-line by the designer in advance without estimation, which is of more practical value.

2. Problem description and preliminaries

In this section, some important concepts of chaotic synchronization will be described in details, and the relevant preliminaries will be listed.

2.1. Vector-polynomial-based synchronization

Consider the nonlinear chaotic synchronization problem among M drive systems and one response system. The dynamics of the j-th basic drive system is described by

$$\begin{cases} \dot{\xi}_{j,1}(t) = Q_{j,1}(\xi_j(t))\varphi_j + q_{j,1}(\xi_j(t)), \\ \dot{\xi}_{j,2}(t) = Q_{j,2}(\xi_j(t))\varphi_j + q_{j,2}(\xi_j(t)), \\ \vdots \\ \dot{\xi}_{j,n}(t) = Q_{j,n}(\xi_j(t))\varphi_j + q_{j,1}(\xi_j(t)), \\ \qquad\qquad j = 1, 2, \cdots, M. \end{cases} \tag{2.1}$$

Correspondingly, the response system is of the form

$$\begin{cases} \dot{w}_1(t) = R_1(w(t))\psi + r_1(w(t)) + u_1(t), \\ \dot{w}_2(t) = R_2(w(t))\psi + r_2(w(t)) + u_2(t), \\ \vdots \\ \dot{w}_n(t) = R_n(w(t))\psi + r_n(w(t)) + u_n(t), \end{cases} \tag{2.2}$$

where $\xi_j = (\xi_{j,1}, \xi_{j,2}, \cdots, \xi_{j,n})^T$ and $w = (w_1, w_2, \cdots, w_n)^T \in R^n$ denote the state vectors for the j-th basic drive system and the response system, respectively, $Q_{j,i}(\xi_j(t))$ and $R_i(w(t))$ denote the i-th rows of the linear functional matrices $Q_j(\xi_j(t))$ and $R(w(t)) \in R^{n\times n}$, respectively, $q_{j,i}(\xi_j(t))$ and $r_i(w(t))$ are continuous nonlinear functions, $\varphi_j = (\varphi_{j,1}, \varphi_{j,2}, \cdots, \varphi_{j,n})^T$ and $\psi = (\psi_1, \psi_2, \cdots, \psi_n)^T \in R^n$ refer to system parameter vectors, the vector $u = (u_1, u_2, \cdots, u_n)^T \in R^n$ is the control input.

Definition 1. *For vector $\upsilon = (\upsilon_1, \upsilon_2, \cdots, \upsilon_n)^T \in R^n$ and constant $l \in Z^+$, a novel $l-th$ power of υ is defined as*

$$\upsilon^{<l>} = (\upsilon_1^l, \upsilon_2^l, \cdots, \upsilon_n^l)^T, \tag{2.3}$$

based on which, a novel vector polynomial with degree $N \in Z^+$ is defined as

$$P_N(\upsilon) = \sum_{l=1}^{N} D_l \upsilon^{<l>}, \tag{2.4}$$

where $D_l = diag\{d_{l,1}, \cdots, d_{l,n}\} \in R^{n\times n}$ denotes the coefficient matrix.

Definition 2. *(Vector-polynomial-based synchronization) The set of chaotic systems (2.1)–(2.2) are said to be vector-polynomial-based synchronization, if*

$$\lim_{t\to\infty} \| \sum_{l=1}^{N} D_l (\sum_{j=1}^{M} A_j \xi_j(t))^{<l>} - \Lambda(t) w(t) \| = 0, \tag{2.5}$$

where A_j and $D_l \in R^{n\times n}$ refer to the coefficient matrices, $\Lambda(t) = diag\{\lambda_1(t), \cdots, \lambda_n(t)\}$ denotes the scaling matrix, whose elements are bounded and continuously differentiable non-zero functions.

Denote

$$\chi(\xi_1, \cdots, \xi_M) = \sum_{j=1}^{M} A_j \xi_j(t),$$

$$P_N(\chi) = \sum_{l=1}^{N} D_l \chi^{<l>}(\xi_1, \cdots, \xi_M),$$

then, (2.5) is reduced to

$$\lim_{t\to\infty} \| P_N(\chi) - \Lambda(t) w(t) \| = 0. \tag{2.6}$$

If this is the case, $P_N(\chi)$ is called a compound drive system.

In order to facilitate the reader to understand, we take the case of $M = 3$ as an example for detailed analysis. In this case, the three basic drive systems are specifically described as

$$\begin{cases} \dot{x}_1(t) = F_1(x(t))\theta + f_1(x(t)), \\ \dot{x}_2(t) = F_2(x(t))\theta + f_2(x(t)), \\ \vdots \\ \dot{x}_n(t) = F_n(x(t))\theta + f_n(x(t)), \end{cases} \tag{2.7}$$

$$\begin{cases} \dot{y}_1(t) = G_1(y(t))\phi + g_1(y(t)) \\ \dot{y}_2(t) = G_2(y(t))\phi + g_2(y(t)) \\ \vdots \\ \dot{y}_n(t) = G_n(y(t))\phi + g_n(y(t)) \end{cases} \tag{2.8}$$

$$\begin{cases} \dot{z}_1(t) = H_1(z(t))\eta + h_1(z(t)), \\ \dot{z}_2(t) = H_2(z(t))\eta + h_2(z(t)), \\ \vdots \\ \dot{z}_n(t) = H_n(z(t))\eta + h_n(z(t)). \end{cases} \tag{2.9}$$

Then, Definition 2 can be rewritten as

Definition 3. *The set of chaotic systems (2.7)–(2.9) and (2.2) are said to be vector-polynomial-based synchronization, if*

$$\lim_{t\to\infty} \| \sum_{l=1}^{N} D_l(Ax(t) + By(t) + Cz(t))^{<l>} - \Lambda(t)w(t)\| = 0. \tag{2.10}$$

Denote

$$\chi(x, y, z) = Ax(t) + By(t) + Cz(t), \tag{2.11}$$

$$P_N(\chi) = \sum_{l=1}^{N} D_l \chi^{<l>}(x, y, z), \tag{2.12}$$

then, (2.10) is reduced to

$$\lim_{t\to\infty} \|P_N(\chi) - \Lambda(t)w(t)\| = 0. \tag{2.13}$$

Remark 4. *As shown in Table 1, the vector-polynomial-based synchronization covers most of the existing chaotic synchronization schemes. The proposed synchronization scheme will be transformed into different specific ones as different parameters are selected. In Table 1,* $\Lambda = diag\{\lambda_1, \cdots, \lambda_n\} \in n\times n$ *refers to a constant diagonal matrix, and* $I \in n \times n$ *denotes a unit matrix.*

Table 1. Comparison among the vector-polynomial-based synchronization and other existing ones.

	Parameter setting	**Name of synchronization scheme**	**Definition of synchronization error**
		Vector-polynomial-based synchronization	$e(t) = \sum_{l=1}^{N} D_l(\sum_{j=1}^{M} A_j\xi_j(t))^{<l>} - \Lambda(t)w(t)$
Case 1	M=3	**Vector-polynomial-based synchronization** with $M = 3$	$e(t) = \sum_{l=1}^{N} D_l(Ax(t) + By(t) + Cz(t))^{<l>} - \Lambda(t)w(t)$
Case 2	$M = 3, N = 1, D = I, C = 0, \Lambda(t) = \Lambda$	**Combined synchronization**	$e(t) = Ax(t) + By(t) - \Lambda w(t)$
Case 3	$M = 3, N = 1, A = D = I, B = C = 0$	**Modified function projective synchronization**	$e(t) = x(t) - \Lambda(t)w(t)$
Case 4	$M = 3, N = 1, A = D = I, B = C = 0, \Lambda(t) = \Lambda$	**Projective synchronization**	$e(t) = x(t) - \Lambda w(t)$
Case 5	$M = 3, N = 1, B = C = 0, A = D = \Lambda(t) = I$	**Complete synchronization**	$e(t) = x(t) - w(t)$
Case 6	$M = 3, N = 1, B = C = 0, A = D = -\Lambda(t) = I$	**Anti-synchronization**	$e(t) = x(t) + w(t)$

Remark 5. *In chaotic secure communication, the more complex the carrier signal is, the stronger the attack resistance of the secure communication scheme is. Definition 3 shows that,* $x(t), y(t)$ *and* $z(t)$ *generate a new vector* $\chi = Ax(t) + By(t) + Cz(t)$ *by linear operation, and then* $\chi(t)$ *generates another vector* $P_N(\chi) = \sum_{l=1}^{N} D_l\chi^{<l>}$ *by polynomial operation. Therefore, the compound vector* $P_N(\chi)$ *has more complex nonlinear features. From the theoretical perspective, the geometric path of the vector-polynomial-based compound drive system* $P_N(\chi((x, y, z)))$ *is more difficult to predict. Moreover, the complexity of* $P_N(\chi((x, y, z)))$ *can be improved by increasing the degree N. Furthermore, different*

compound drive systems can be obtained by selecting different coefficient matrices D_l for the fixed $\chi(x, y, z)$ and N, which indicates the synchronization scheme (2.10) is more flexible.

For instance, when we select the following three sets of different coefficient matrices for the basic drive systems (2.7)–(2.9), the corresponding 3D projections of the vector-polynomial-based compound drive system $P_N(\chi((x, y, z)))$ are shown in Figure 2(a),(b) and (c), respectively.

Case a:

$$D_1 = 10^{-5} \cdot diag\{-20, -6, 3\},$$
$$D_2 = 10^{-5} \cdot diag\{-5, 9, 10\},$$
$$D_3 = 10^{-5} \cdot diag\{3, 0.5, -8\},$$

Case b:

$$D_1 = 10^{-5} \cdot diag\{-5, 12, 6\},$$
$$D_2 = 10^{-5} \cdot diag\{-4, 2, 2\},$$
$$D_3 = 10^{-5} \cdot diag\{10, -3, 1\},$$

Case c:

$$D_1 = 10^{-5} \cdot diag\{5, 1, -10\},$$
$$D_2 = 10^{-5} \cdot diag\{16, -6, 5\},$$
$$D_3 = 10^{-5} \cdot diag\{4, -8, 2\}.$$

The comparison of Figures 1 and 2 shows that, the chaotic topology of the compound system is more complex than that of the three basic drive systems.

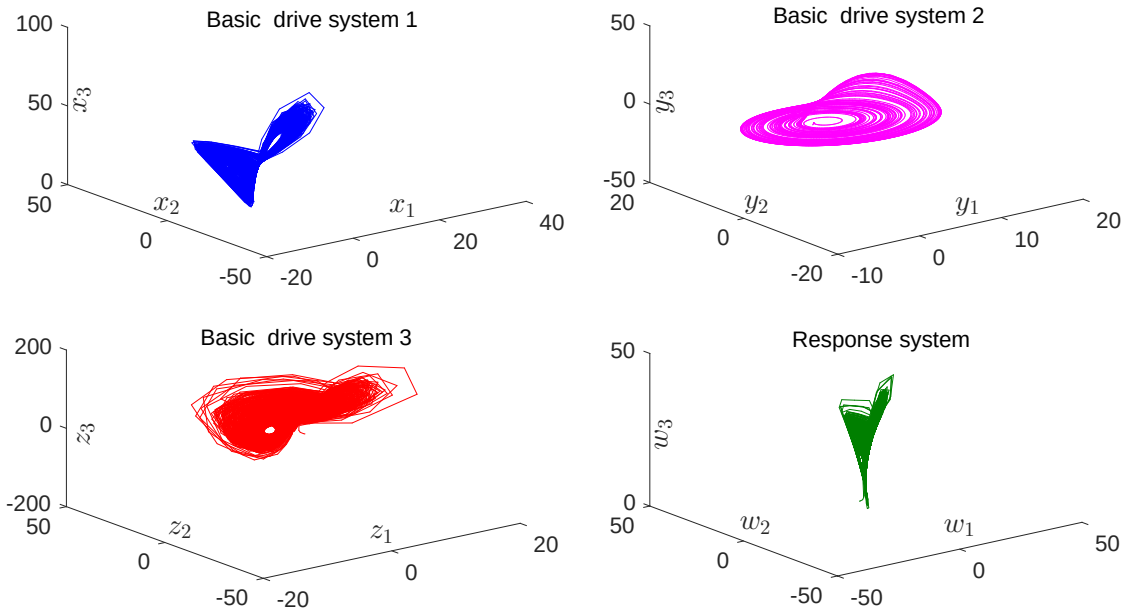

Figure 1. 3D projections of the four chaotic systems involved in the simulations of this work.

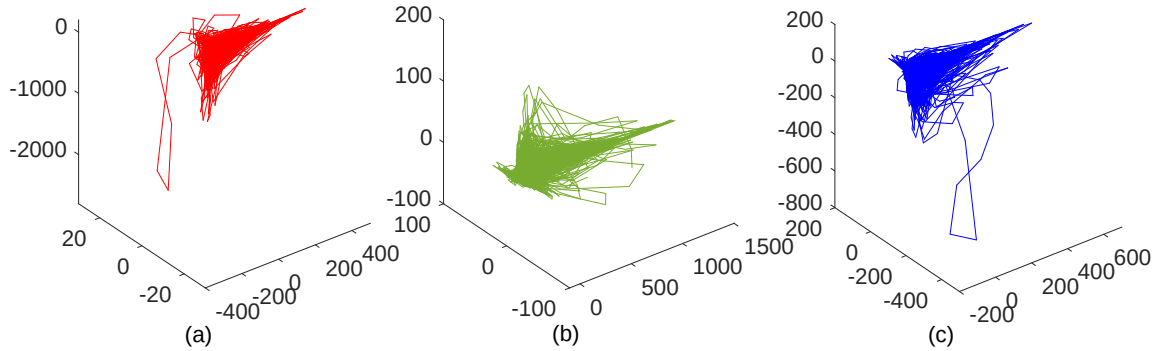

Figure 2. 3D projections of the vector-polynomial-based compound drive system with different coefficient matrices.

Denote the synchronization error among the set of chaotic systems (2.7)–(2.9) and (2.2) as below:

$$e(t) = P_N(\chi) - \Lambda(t)w(t),$$

or

$$e_i(t) = P_{N,i}(\chi) - \lambda_i(t)w_i(t) = \sum_{l=1}^{N} d_{l,i}\chi_i^l - \lambda_i(t)w_i(t)$$

where

$$\chi_i = A_i x(t) + B_i y(t) + C_i z(t),$$

A_i, B_i,and C_i denote the ith row of the matrixes A, B and C, respectively. $i = 1, 2, \cdots, n$.

Since

$$\begin{aligned}\dot{\chi}_i &= A_i\dot{x}(t) + B_i\dot{y}(t) + C_i\dot{z}(t)\\ &= A_i(F(x)\theta + f(x)) + B_i(G(y)\phi + g(y)) + C_i(H(z)\eta + h(z)),\end{aligned}$$

it follows that

$$\dot{P}_{N,i}(\chi) = \sum_{l=1}^{N} l d_{l,i}\chi_i^{l-1}\dot{\chi}_i = \sum_{l=1}^{N} l d_{l,i}\chi_i^{l-1}(A_i\dot{x}(t) + B_i\dot{y}(t) + C_i\dot{z}(t)).$$

Then, the error dynamic system among the chaotic systems (2.7)-(2.9) and (2.2) is obtained as below

$$\dot{e}_i(t) = \dot{P}_{N,i}(\chi) - \dot{\lambda}_i w_i(t) - \lambda_i\dot{w}_i(t), \tag{2.14}$$

that is

$$\begin{aligned}\dot{e}_i(t) = &\sum_{l=1}^{N} l d_{l,i}\chi_i^{l-1}(A_i(F(x)\theta + f(x)) + B_i(G(y)\phi + g(y)) + C_i(H(z)\eta + h(z)))\\ &- \dot{\lambda}_i w_i(t) - \lambda_i(R_i(w)\psi + r_i(w)) - \lambda_i u_i(t).\end{aligned} \tag{2.15}$$

2.2. Predefined-time vector-polynomial-based synchronization

Before defining the concept of predefined-time synchronization, let us review some related concepts and properties.

Consider the nonlinear dynamical system

$$\dot{\xi}(t) = \vartheta(t, \xi; \varphi), t \in [0, +\infty) \tag{2.16}$$

in which $\chi \in R^n$ represents the system state, $\varphi \in R^m$ denotes the system parameter. The origin $0 \in R^n$ is assumed to be an equilibrium point for the system (2.16), i.e., $\vartheta(0, \xi_0; \varphi) = 0$. The initial condition is represented as $\xi_0 = \xi(0)$.

Definition 6. *(***Predefined-time stability***) [26]. For a predefined constant $T^* > 0$, the origin of (2.16) is said to be globally predefined-time stable, if it holds for all the initial states ξ_0 that*

$$\begin{cases} \lim\limits_{t \to T_-^*} \xi(t, \xi_0) = 0, \quad t \in [0, T^*) \\ \xi(t, \xi_0) \equiv 0, t \in [T^*, +\infty) \end{cases} \tag{2.17}$$

If this is the case, T^* is called a predefined time.

Remark 7. *As shown in Table 2, for the four stabilities involved, the accuracy of the settling-time is gradually enhanced in turn, and the predefined-time stability can be regarded as a upgrade of the other three. Furthermore, the settling-time T^* for predefined-time stability can be pre-specified without being affected by the initial condition ξ_0 or other system parameter φ, thus it can be set freely and has more practical value.*

Table 2. Comparison among the predefined-time stability and other existing ones.

Concept	Definition	Characteristic
Asymptotically stability	The origin of system (2.16) complies with $\lim\limits_{t \to \infty} \xi(t, \xi_0) = 0.$	The length of the stabilization time is unknown and may be infinite.
Finite-time stability [17]	The origin of system (2.16) is globally asymptotically stable and there exists a finite time $T(\xi_0) \geq 0$ satisfying $\begin{cases} \lim\limits_{t \to T(\xi_0)-} \xi(t, \xi_0) = 0, & t \in [0, T(\xi_0)) \\ \xi(t, \xi_0) \equiv 0, & t \in [T(\xi_0), +\infty) \end{cases}$	The stabilization time $T(\xi_0)$ is finite, but is dependent on ξ_0 and the upper bound cannot be estimated.
Fixed-time stability [23]	The origin of system (2.16) is finite-time stable and the settling-time function $T(\xi_0)$ is bounded, i.e., there exists a finite positive constant T_f such that $T(\xi_0) \leq T_f, \forall \xi_0 \in R^n.$	T_f is independent of ξ_0, however, it still depends on the control gains.
Predefined-time stability proposed in this work	The origin of system (2.16) is fixed-time stable and for an predefined time $T^* \geq 0$, it holds that $\begin{cases} \lim\limits_{t \to T^*-} \xi(t, \xi_0) = 0, & t \in [0, T^*) \\ \xi(t, \xi_0) \equiv 0, & t \in [T^*, +\infty) \end{cases}, \forall \xi_0 \in R^n.$	T^* can be predefined and not affected by ξ_0 or other control gains.

Lemma 8. *[24] For the dynamic system (2.16), if there exists a radially unbounded Lyapunov function $V : R^n \to R$ that complies to*

$$\dot{V} \leq -(\mu_1 V^{\varepsilon_1} + \mu_2 V^{\varepsilon_2}), \xi \in R^n \setminus 0$$

where $\mu_1 \in (0, +\infty)$, $\mu_2 \in (0, +\infty)$, $\varepsilon_1 \in (1, +\infty)$ and $\varepsilon_2 \in [0, 1)$ are given constants.

Then, the origin of system (2.16) is fixed-time stable and an upper bound of settling-time function $T(\xi_0)$ is estimated as

$$T_f = \frac{1}{\mu_1(\varepsilon_1 - 1)} + \frac{1}{\mu_2(1 - \varepsilon_2)}, \forall \xi_0 \in R^n \setminus 0. \tag{2.18}$$

Remark 9. *From Lemma 8 one can see that, for the fixed-time stability, the the upper bound T_f of the setting-time function $T(\xi_0)$ does not depend on the initial condition. Nevertheless, the relationship between T_f and the control gains is unclear. For several engineering application, such as chaos synchronization, it is required that the synchronization time can be set independently as a user-defined parameter.*

Lemma 10. *[27] Let $T^* > 0$ be a predefined constant. If there exists a radially unbounded Lyapunov function $V : R^n \to R$ for the system (2.16), such that*

$$\dot{V} \leq -\frac{1}{\alpha T^*} \exp(V^\alpha) V^{1-\alpha}, \ \ \alpha \in (0, 1],$$

for any $\xi \in R^n \setminus 0$.

Then, the origin of system (2.16) is predefined-time stable with T^* as the predefined time.

Combining the concepts of predefined-time stability and vector-polynomial-based synchronization, now we propose the following important definition.

Definition 11. *(***Predefined-time vector-polynomial-based synchronization***) The set of chaotic systems (2.7)–(2.9) and (2.2) are said to be predefined-time vector-polynomial-based synchronization, if the origin of the synchronization error system (2.15) is predefined-time stable with $T^* > 0$ as the predefined time, i.e.,*

$$\begin{cases} \lim\limits_{t \to T^*_-} e_i(t) = 0, \ \ t \in [0, T^*) \\ e_i(t) \equiv 0, t \in [T^*, +\infty) \end{cases} \tag{2.19}$$

where $i = 1, 2, \cdots, n$.

In this case, T^* is called the predefined synchronization time.

3. Design of the predefined-time synchronization controller

To realize the predefined-time vector-polynomial-based synchronization among the set of chaotic systems (2.7)–(2.9) and (2.2), the following synchronization controller is designed,

$$\begin{aligned} u_i(t) = & \frac{1}{\lambda_i(t)} \left(\frac{1}{2^{1-\alpha} \alpha T^*} \exp\left(\frac{e_i(t)^{2\alpha}}{2^\alpha} \right) \text{sign}(e_i(t)) |e_i|^{1-2\alpha} + \Omega_i \right) \\ & i = 1, 2, \cdots, n. \end{aligned} \tag{3.1}$$

in which, T^* is the tunable predefined synchronization time, $\alpha \in (0, 0.5) \cup (0.5, 1]$ is a control parameter,

$$\begin{aligned} \Omega_i = & \sum_{l=1}^{N} l d_{l,i} \chi_i^{l-1} (A_i(F(x)\theta + f(t)) + B_i(G(y)\phi + g(y)) + C_i(H(z)\eta + h(z))) \\ & - \lambda_i(t)(R_i(w)\psi + r_i(w)) - \dot{\lambda}_i(t) w_i(t). \end{aligned} \tag{3.2}$$

Theorem 12. *If the synchronization controller (3.1) is adopted, then the predefined-time vector-polynomial-based synchronization among the set of chaotic systems (2.7)–(2.9) and (2.2) will be achieved with $T^* > 0$ as the predefined synchronization time.*

Proof. Choose the following Lyapunov function

$$V_i(t) = \frac{1}{2}e_i^2(t), i = 1, 2, \cdots, n. \tag{3.3}$$

According to the definition of Ω_i, the synchronization error dynamic system (2.15) can be simplified as

$$\dot{e}_i(t) = \Omega_i - \lambda_i(t)u_i(t). \tag{3.4}$$

Taking the derivative of $V_i(t)$ along (2.15) , it can be derived that

$$\begin{aligned}
\dot{V}_i(t) &= e_i(t)\dot{e}_i(t) \\
&= e_i(t)(\Omega_i - \lambda_i(t)u_i(t)) \\
&= e_i(t)(\Omega_i - \frac{1}{2^{1-\alpha}\alpha T^*}\exp(\frac{e_i^{2\alpha}}{2^\alpha})\text{sign}(e_i(t))|e_i(t)|^{1-2\alpha} - \Omega_i) \\
&= -\frac{1}{2^{1-\alpha}\alpha T^*}\exp(\frac{e_i(t)^{2\alpha}}{2^\alpha})|e_i(t)|^{2-2\alpha} \\
&= -\frac{1}{\alpha T^*}\exp(V_i^\alpha)V_i^{1-\alpha}.
\end{aligned} \tag{3.5}$$

Hence, it follows from Lemma 10 that each element $e_i(t)$ of the synchronization error vector $e(t)$ will converge to zero before the predefined time T^*, which means the predefined-time vector-polynomial-based synchronization among the chaotic systems (2.7)–(2.9) and (2.2) will be achieved with T^* as the predefined synchronization time. □

Similarly, if we define the synchronization error among the $M + 1$ chaotic systems (2.1) and (2.2) as

$$e(t) = P_N(\chi) - \Lambda(t)w(t) = \sum_{l=1}^{N} D_l\chi^{<l>}(x_1, \cdots, x_M) - \Lambda(t)w(t), \tag{3.6}$$

in which, $\chi(x_1, \cdots, x_M) = \sum\limits_{j=1}^{M} A_j x_j(t)$.

Then the result of Theorem 12 can be generalized as below.

Theorem 13. *For a predefined time $T^* > 0$, if the following synchronization controller is adopted*

$$\begin{aligned}
u_i(t) &= \frac{1}{\lambda_i(t)}(\frac{1}{2^{1-\alpha}\alpha T^*}\exp(\frac{e_i(t)^{2\alpha}}{2^\alpha})\text{sign}(e_i(t))|e_i(t)|^{1-2\alpha} + \Omega_i),\ \alpha \in (0, 0.5) \cup (0.5, 1] \\
i &= 1, 2, \cdots, n,
\end{aligned} \tag{3.7}$$

in which

$$\Omega_i = \sum_{l=1}^{N} ld_{l,i}\chi_i^{l-1}(\sum_{j=1}^{M}(A_{j,i}(F_j(x_j)\theta_j + f_j(t))) - \dot{\lambda}_i(t)w_i(t) - \lambda_i(t)(R_i(w)\psi + r_i(w)), \tag{3.8}$$

χ_i and $e_i(t)$ refer to the i-th elements of vectors $\chi(x_1, \cdots, x_M)$ and $e(t)$, respectively, $A_{j,i}$ represents the i-th row of the matrix A_j.

Then, the predefined-predefined vector-polynomial-based synchronization among the $M+1$ chaotic systems (2.1) and (2.2) will be achieved with T^* as the predefined synchronization time.

Proof. The proof process is similar to that of Theorem 12 and is omitted here. □

4. Numerical simulation

In this section, an illustrative numerical example is given to highlight the properties of the chaotic synchronization scheme and synchronization control technology. The chaotic systems involved in this example are given as below.

The first basic drive system (**Lorenze system**)

$$\begin{pmatrix} \dot{x}_1 \\ \dot{x}_2 \\ \dot{x}_3 \end{pmatrix} = \underbrace{\begin{pmatrix} x_2 - x_1 & 0 & 0 \\ 3x_1 & x_2 & 0 \\ 0 & 0 & x_3 \end{pmatrix}}_{F(x(t))} \underbrace{\begin{pmatrix} 10 \\ -1 \\ -8/3 \end{pmatrix}}_{\theta} + \underbrace{\begin{pmatrix} 0 \\ -x_1x_3 \\ x_1x_2 \end{pmatrix}}_{f(x(t))}, \tag{4.1}$$

The second basic drive system (**Rössler system**)

$$\begin{pmatrix} \dot{y}_1 \\ \dot{y}_2 \\ \dot{y}_3 \end{pmatrix} = \underbrace{\begin{pmatrix} -y_2 - y_3 & 0 & 0 \\ y_1 & y_2 & 0 \\ 0 & 0 & -y_3 \end{pmatrix}}_{G(y(t))} \underbrace{\begin{pmatrix} 1 \\ 0.2 \\ 5.7 \end{pmatrix}}_{\phi} + \underbrace{\begin{pmatrix} 0 \\ 0 \\ y_1y_3 + 0.2 \end{pmatrix}}_{g(y(t))}, \tag{4.2}$$

The third basic drive system (**Liu system**)

$$\begin{pmatrix} \dot{z}_1 \\ \dot{z}_2 \\ \dot{z}_3 \end{pmatrix} = \underbrace{\begin{pmatrix} z_2 - z_1 & 0 & 0 \\ 0 & z_1 & 0 \\ 0 & 0 & -z_3 \end{pmatrix}}_{H(z(t))} \underbrace{\begin{pmatrix} 10 \\ 40 \\ 2.5 \end{pmatrix}}_{\eta} + \underbrace{\begin{pmatrix} 0 \\ -z_1z_3 \\ 4z_1^2 \end{pmatrix}}_{h(z(t))}, \tag{4.3}$$

The response system (**Lü system**)

$$\begin{pmatrix} \dot{w}_1 \\ \dot{w}_2 \\ \dot{w}_3 \end{pmatrix} = \underbrace{\begin{pmatrix} w_2 - w_1 & 0 & 0 \\ 0 & w_2 & 0 \\ 0 & 0 & -w_3 \end{pmatrix}}_{R(w(t))} \underbrace{\begin{pmatrix} 36 \\ 20 \\ 3 \end{pmatrix}}_{\psi} + \underbrace{\begin{pmatrix} 0 \\ -w_1w_3 \\ w_1w_2 \end{pmatrix}}_{r(w(t))}. \tag{4.4}$$

When the initial states are set as $x(0) = (0.1, 0.1, 0.1)^T$, $y(0) = (-1, 1, -2)^T$, $z(0) = (2, 0.5, -1)^T$ and $w(0) = (-1.2, 2, 4)^T$, the project curves of the above four chaotic systems are shown in Figure 1.

According to Definition 11, the predefined-time synchronization objective in this simulation can be described as

$$\begin{cases} \lim\limits_{t \to T^*-} \|e(t)\| = \lim\limits_{t \to T^*-} \|P_N(\chi) - \Lambda(t)w(t)\|, & \text{if } t < T^* \\ \|e(t)\| = \|P_N(\chi) - \Lambda(t)w(t)\| \equiv 0, & \text{if } t \geq T^* \end{cases} \tag{4.5}$$

where $T^* > 0$ denotes the predefined synchronization time, $\chi = Ax(t) + By(t) + Cz(t)$ refers to a combined chaotic system generated by the three basic drive systems with the following combined coefficients,

$$A = \begin{pmatrix} 1 & 2 & 3 \\ 2 & -1 & -2 \\ 3 & 0 & -2 \end{pmatrix},$$
$$B = \begin{pmatrix} -2 & 0.2 & 1 \\ 0 & 3 & 1 \\ 4 & 1 & 3 \end{pmatrix},$$
$$C = \begin{pmatrix} 2 & 3 & 0 \\ 0.2 & 0.5 & 1.5 \\ 1 & -2.5 & 2 \end{pmatrix}.$$

Meanwhile, the coefficient matrices in $P_N(\chi)$ and the synchronization scaling matrix are taken as

$$\begin{aligned} D_1 &= diag\{-8, -8, -8\}, \\ D_2 &= diag\{0.2, 0.2, 0.2\}, \\ D_3 &= diag\{2 \times 10^{-5}, 2 \times 10^{-5}, 2 \times 10^{-5}\}, \\ \Lambda(t) &= diag\{2 - 0.5\cos t, 1 - 0.4\sin 2t, -2 + \cos 3t\}. \end{aligned}$$

When the simulation time is taken as 400 seconds, the phase portraits of the combined chaotic signal $Ax + By + Cz$ and the compound chaotic signal $P_N(Ax + By + Cz)$ are displayed in Figure 3. Comparing Figure 3 with Figure 1, it is appreciable that, the trajectory of the compound chaotic signal $P_N(Ax + By + Cz)$ is more complex.

Now we appoint the predefined synchronization time as $T^* = 0.1$, and carry out the chaotic synchronization simulation under the predefined-time synchronization controller (3.1) with $\alpha = 0.2$. The simulation result displayed by Figure 4 implies that, the synchronization error $e_i(t)$ converges to zero before the predefined time $T^* = 0.1$, which shows the effectiveness of the proposed synchronization control technique.

Subsequently, we reset the predefined synchronization time T^* to 0.01 and carry out the predefined-time synchronization simulation again. As shown in Figure 5, the synchronization among the chaotic systems (4.1)–(4.4) is still achieved successfully before the predefined time $T^* = 0.01$, which verifies the flexibility of the proposed predefined-time synchronization controller.

Next, we replace the predefined-time controller (3.1) in the above chaotic synchronization simulation with the following fixed-time controller presented in [24],

$$\bar{u}_i(t) = \frac{1}{\lambda_i(t)}(\Omega_i + \frac{\mu_1 \text{sign}(e_i(t))|e_i(t)|^{2\varepsilon_1 - 1}}{2^{\varepsilon_1}} + \frac{\mu_2 \text{sign}(e_i(t))|e_i(t)|^{2\varepsilon_2 - 1}}{2^{\varepsilon_2}}), \quad i = 1, 2, \cdots, n \tag{4.6}$$

where $\varepsilon_1 = 1.1$, $\varepsilon_2 = 0.9$, $\mu_1 = 2$, $\mu_2 = 3$, and Ω_i is defined by (3.2).

Constructing the following Lyapunov function

$$\bar{V}_i(t) = \frac{1}{2} {e_i}^2(t),$$

it can be derived

$$\dot{\bar{V}}_i \leq -(\mu_1(\bar{V}_i)^{\varepsilon_1} + \mu_2(\bar{V}_i)^{\varepsilon_2}).$$

By virtue of Lemma 8, the synchronization among chaotic systems (4.1)–(4.4) can be achieved. The corresponding simulation result is shown in Figure 6. Comparing Figure 6 with Figures 4 and 5, one can see that, the synchronization accuracy and synchronization rate under the fixed-time controller (4.6) are obviously inferior to that under the predefined-time controller. This further verifies the superiority of the proposed predefined-time synchronization control technique.

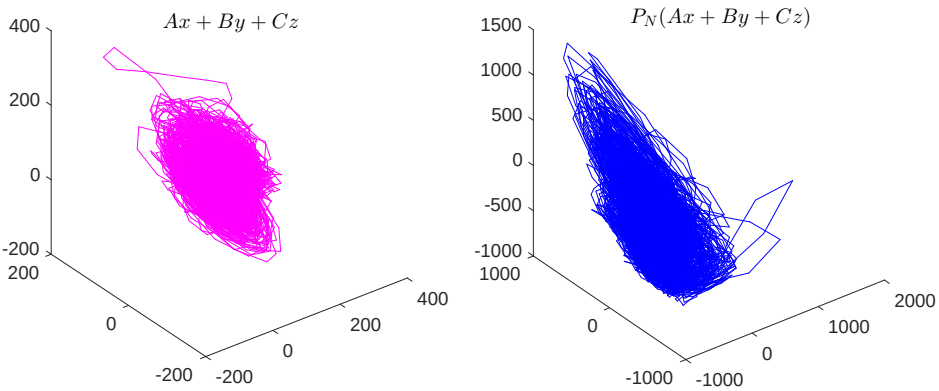

Figure 3. 3D phase portraits of the vector-polynomial-function-based drive system.

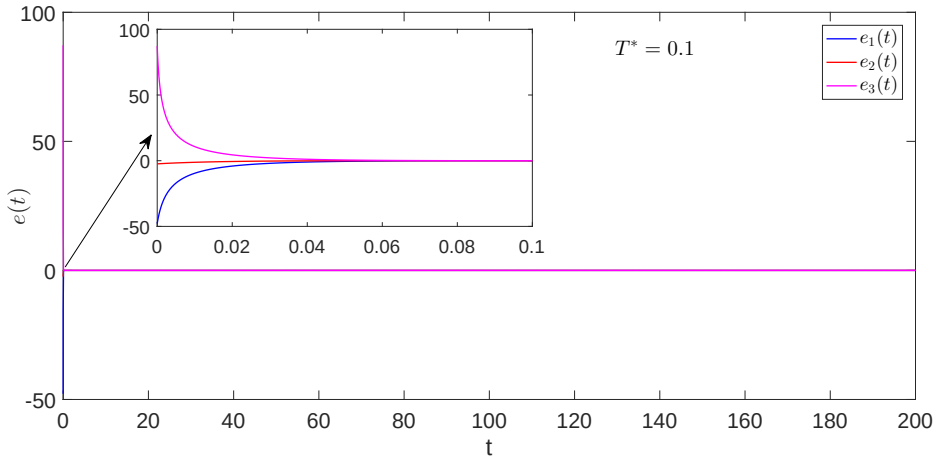

Figure 4. Trajectory of the synchronization error via predefined-time control technique with $T^* = 0.1$.

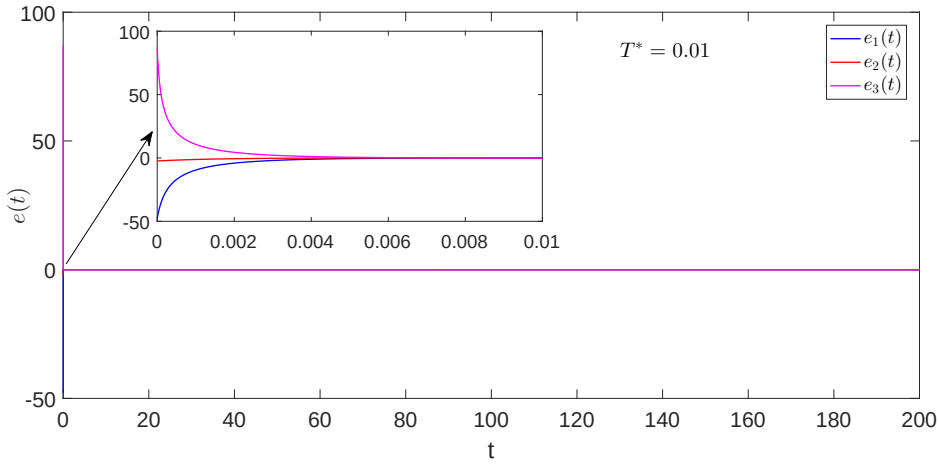

Figure 5. Trajectory of the synchronization error via predefined-time control technique with $T^* = 0.01$.

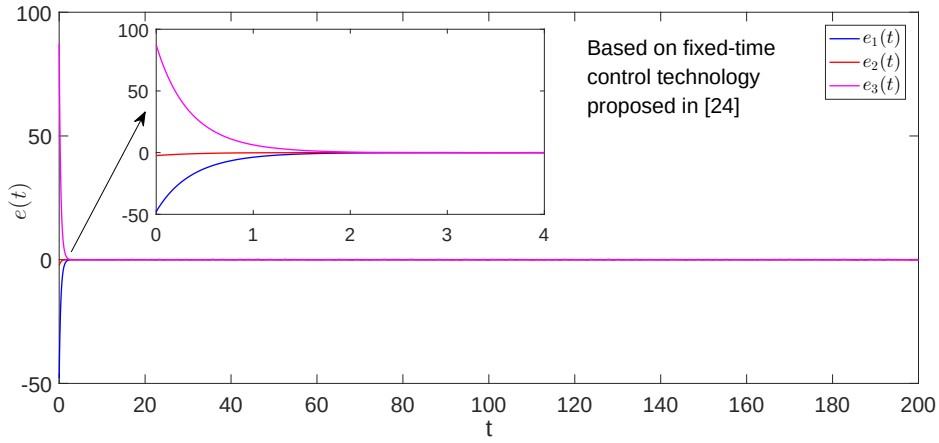

Figure 6. Trajectory of the synchronization error via fixed-time control technique.

5. Applied experiments in chaotic secure communication based on the proposed synchronization scheme

In this section, several chaotic secure communication experiments will be carried out to illustrate the feasibility of the proposed synchronization scheme.

The chaotic systems, synchronization schemes, synchronization control techniques and related parameters involved in the following experiments are the same as those given in Section 4. Meanwhile, the predefined synchronization time is set to $T^* = 0.01$.

5.1. Application in chaotic secure transmission of dynamic signal

The framework of chaotic secure transmission of dynamic signal is depicted by Figure 7, while the corresponding communication principle is explained as follows:

At the sender end, chaotic signals $x(t), y(t)$ and $z(t)$ generate a new chaotic signal $P_N(\chi(x, y, z))$ as the carrier signal by means of algebraic polynomial operation. Subsequently, according to the specified encryption scheme, the carrier signal $P_N(\chi(x, y, z))$ and the original signal $s(t)$ are modulated into another nonlinear signal $m(t)$, which will be transmitted through the transmission channel. At the receiver end, the receiver realizes the predefined-time synchronization among the response and the drive systems via the controller $u(t)$ and further reverses the carrier signal as $\hat{P}_N(\chi(x, y, z))$. Finally, the original signal is recovered as $\hat{s}(t)$ via the decryption scheme.

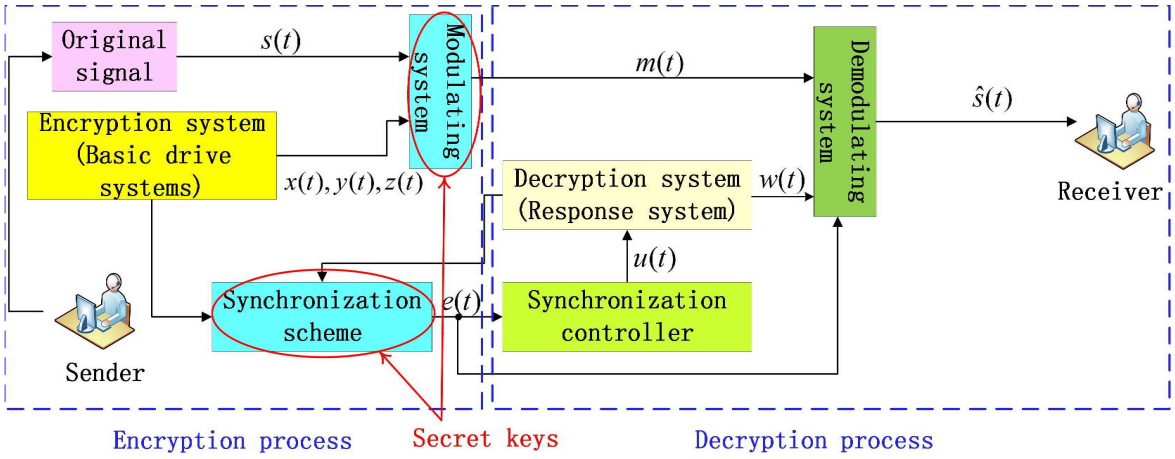

Figure 7. Framework of the chaotic secure transmission of dynamic signal.

The original dynamic signal in this simulation experiment is given as

$$s(t) = \begin{cases} 0, & t \in [2(k-1), 2k-1) \\ 5, & t \in [2k-1, 2k) \end{cases}, k = 1, 2, \cdots.$$

During the encryption process, the signal modulation scheme is designed as

$$m(t) = s(t) + \kappa P_N(\chi(x, y, z)), \tag{5.1}$$

where $\kappa = (0.1, 0.2, -0.1)^T$.

As shown in Figure 8, the encrypted signal $m(t)$ based on the signal modulation scheme (5.1) is more complex and more difficult to predict than the original signal $s(t)$, which indicates that the original signal can be well hidden during the transmission process.

During the decryption process, the following decrypted signal is obtained by using the secret keys including the signal modulation scheme (5.1) and the chaotic synchronization scheme (4.5)

$$\hat{s}(t) = m(t) - \kappa \hat{P}_N(\chi(x, y, z)), \tag{5.2}$$

where $\hat{P}_N(\chi(x, y, z) = \Lambda(t)w(t)$.

As shown in Figure 9, the decrypted dynamic signal $\hat{s}(t)$ can restore the original dynamic signal $s(t)$ accurately as $t \geq T^* = 0.01$.

Meanwhile, comparing Figure 9 with the simulation result (shown in Figure 10) based on the fixed-time synchronization controller (4.6), one can see that, the decoding time under the proposed

predefined-time synchronization scheme is much shorter. Moreover, the decoding time via the proposed predefined-time synchronization control scheme can be set in advance according to the user's requirements, so it is more flexible.

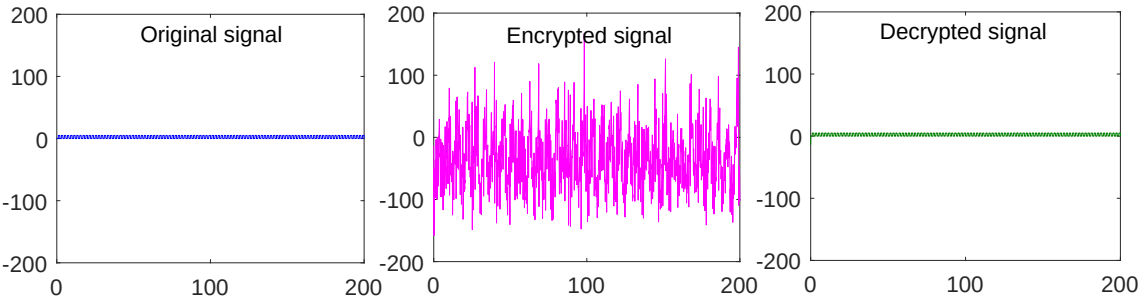

Figure 8. Comparison among the original, encrypted and decrypted signal via predefined-time control technique with $T^* = 0.01$.

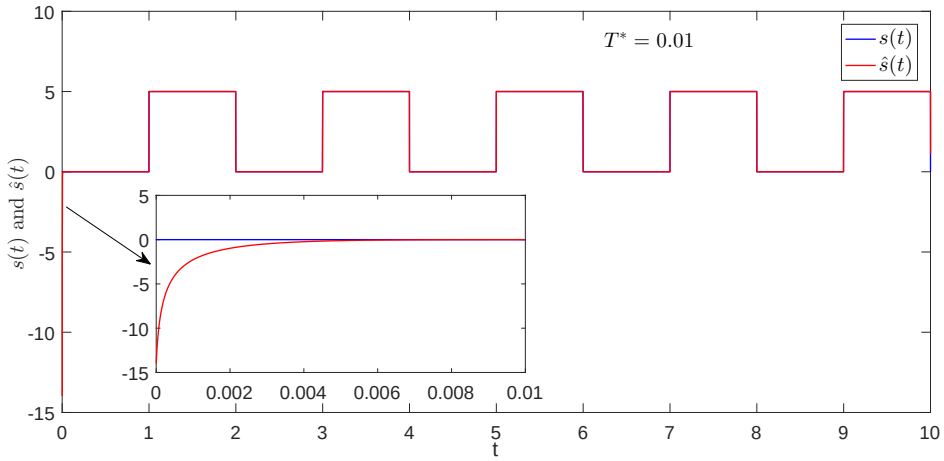

Figure 9. State trajectories of the original signal $s(t)$ and the decrypted signal $\hat{s}(t)$ via predefined-time control technique with $T^* = 0.01$.

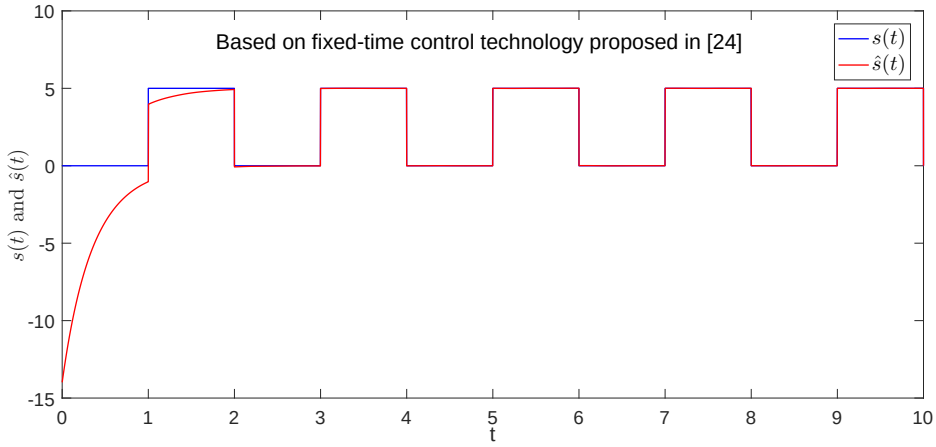

Figure 10. State trajectories of the original signal $s(t)$ and the decrypted signal $\hat{s}(t)$ via fixed-time control technique.

5.2. Application in chaotic secure image transmission

The framework of chaotic secure image transmission based on the proposed chaotic synchronization scheme is shown in Figure 11. The corresponding image encryption algorithms for the black-white image and the color image are described by Algorithm 1 and Algorithm 2, respectively. In the process of the chaotic secure image transmission, the discrete chaotic sequences applied in Algorithm 1 and Algorithm 2 are coded by

$$\begin{aligned} a1(i) &= |P1((1000+i)h)|, \\ a2(i) &= |P1((1200+i)h)|, \\ b1(i) &= |P2((1000+i)h)|, \\ b2(i) &= |P2((1200+i)h)|, \end{aligned}$$

and

$$\begin{aligned} c1(i) &= |P1((500+i)h)|, \\ c2(i) &= |P1((1000+i)h)|, \\ d1(i) &= |P2((500+i)h)|, \\ d2(i) &= |P2((1000+i)h)|, \end{aligned}$$

in which, $h = 0.001$ is the sampling interval, $P1(t) = \kappa P_N \chi(x(t), y(t), z(t))$, $P2(t) = \kappa \Lambda(t) w(t)$, $\kappa = (0.1, 0.2, -0.1)^T$, and $i = 1, 2, \cdots, M \cdot N$.

During the secure image transmission process, the black-white image (Figure12(a)) and the color image (Figure12(a)) of the famous image named Lena are selected as the original images, respectively. The simulation results are shown in Figures 12–14, from which one can see that, high precision image security transmission is realized between the generator and the receiver via the proposed predefined-time chaotic synchronization scheme.

As shown in Figures 15 and 16, when the predefined-time controller (3.1) applied in the above image transmission scheme is replaced by the fixed-time controller (4.6), the encrypted image can not

be successfully recovered. This further proves the validity and superiority of the proposed predefined-time chaotic synchronization control technique.

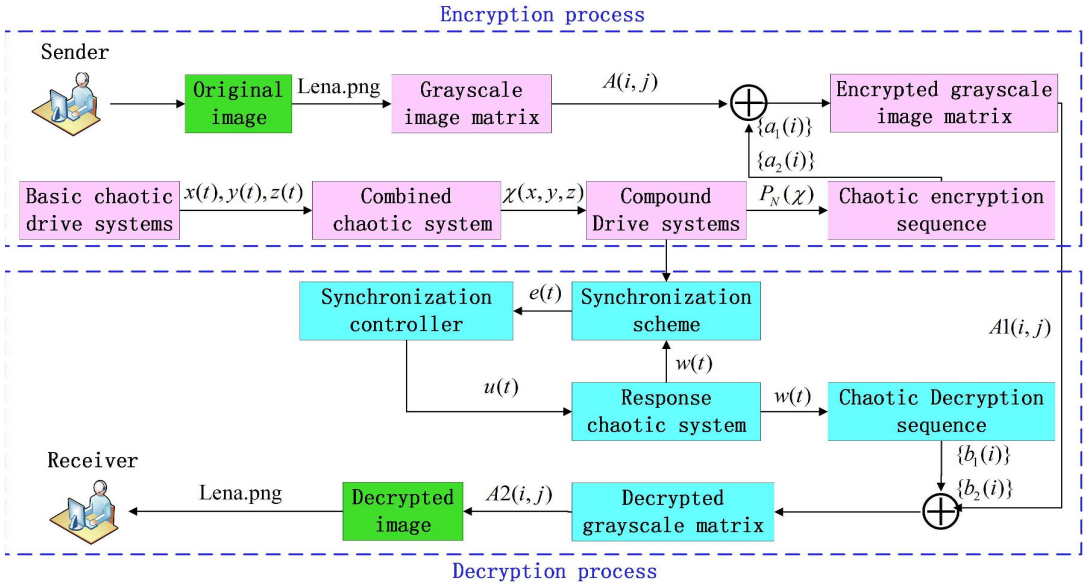

Figure 11. Framework of the chaotic secure image transmission.

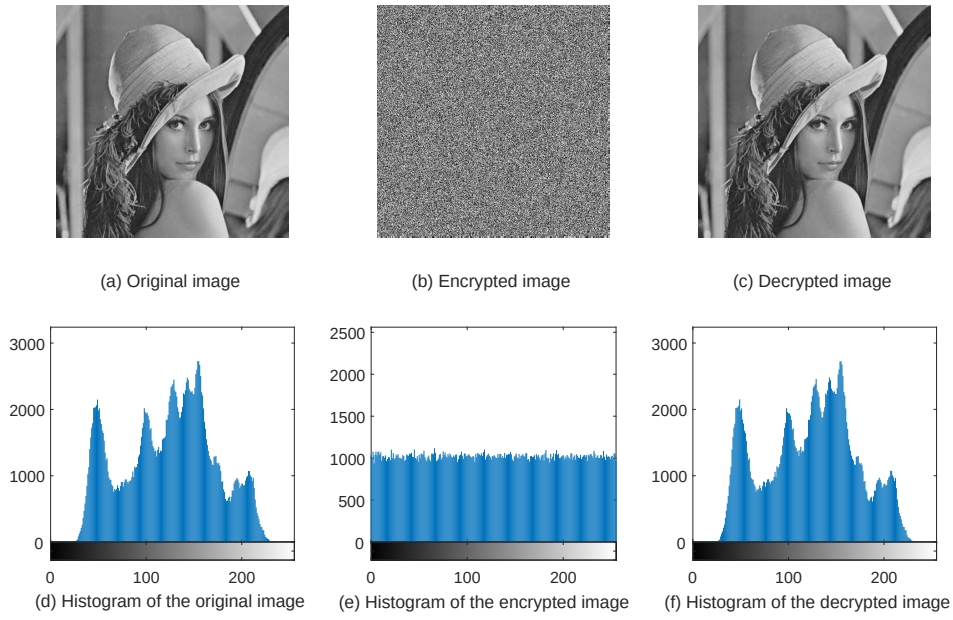

Figure 12. Original image, encrypted image, decrypted image and their histograms of the black-white image with $T^* = 0.01$.

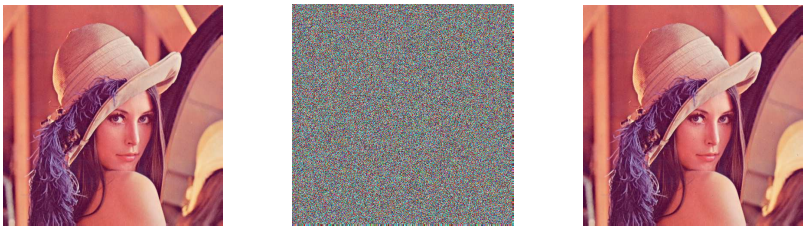

(a) Original image (b) Encrypted image (c) Decrypted image

Figure 13. Original image, encrypted image, and decrypted image of the colour image with $T^* = 0.01$.

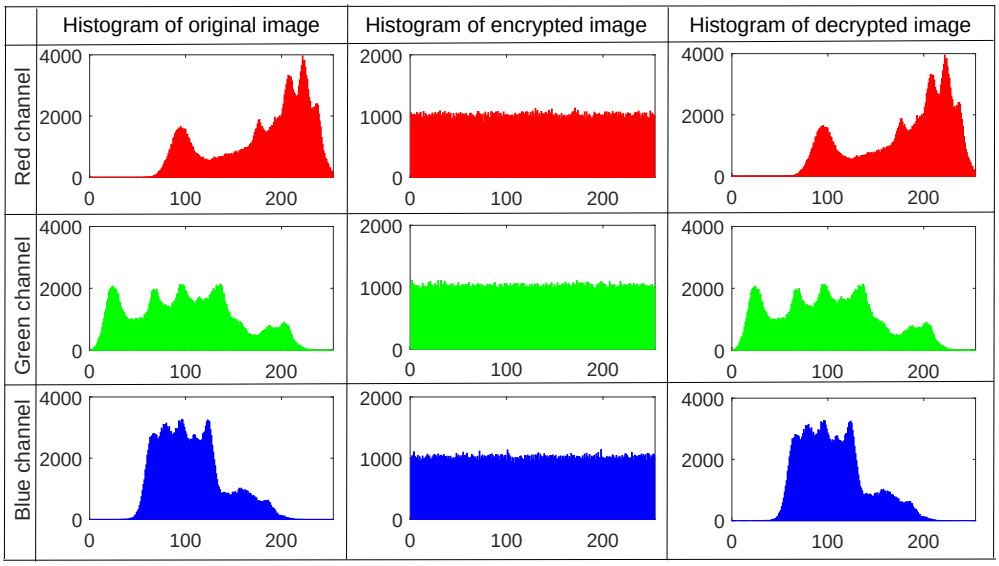

Figure 14. Histograms of original image, encrypted image, and decrypted image of the colour image via fixed-time control technology.

Based on fixed-time control technology proposed in [24]

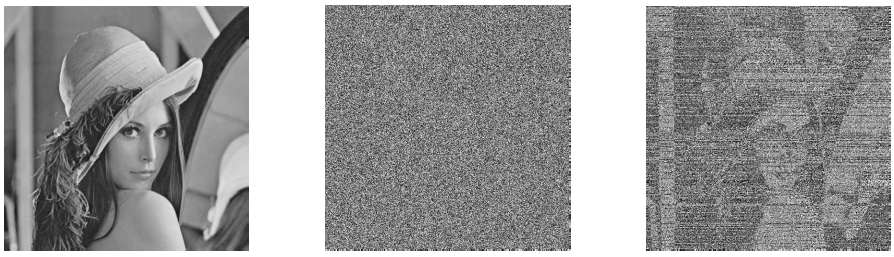

(a) Original image (b) Encrypted image (c) Decrypted image

Figure 15. Original image, encrypted image, decrypted image and their histograms of the black-white image via fixed-time control technology.

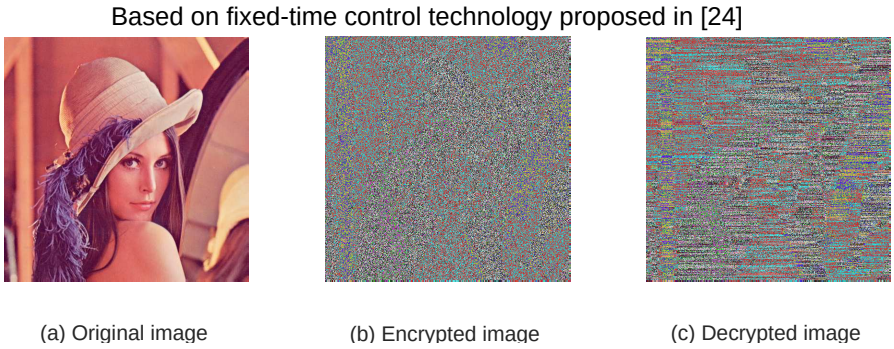

Figure 16. Original image, encrypted image, and decrypted image of the colour image via fixed-time control technology.

6. Conclusions

In this work, a novel predefined-time vector-polynomial-based synchronization scheme for multiple chaotic systems has been proposed and applied in the secure communication of digital signal and image. Both the theoretical and experimental results indicated that, the proposed synchronization scheme can improve the anti-decoding ability of the chaotic secure communication significantly, meanwhile the designed synchronization control technique can improve the decoding speed of the secure transmission effectively. Reliable control and sample-date control are two novel and effective control techniques [19, 20]. Therefore, in our future works, we will consider combining the above control methods with the predefined-time control technique to design two new control techniques "predefined-time reliable control" and "predefined-time sample-date control", which will be meaningful. In addition, it will be also interesting to extend the results in this work to the fractional-order chaotic systems.

Acknowledgments

The research is supported by the National Natural Science Foundation of China with Grant No. 61877046,the Key Science and Technology Projects in Henan Province with Grant No. 212102210552, and the Key Scientific Research Projects of Higher Education Institutions in Henan Province with Grant No. 19B110006. Thanks for the editor and reviewers.

Conflict of interest

The authors declare that there is no conflict of financial interests regarding the publication of this paper.

Algorithm 1 Black-white image encryption algorithm based on the proposed chaotic synchronization scheme.

```
A=imread('lena2.png');
[M,N,L]=size(A);
imshow(A);
A0=A;
% Encryption process:
Rm = randsample(M,M)';
Mchange = [1:1:M;Rm];
Rn = randsample(N,N)';
Nchange = [1:1:N;Rn];
A (Mchange(1,:),:) = A (Mchange(2,:),:);
A (:,Nchange(1,:)) = A (:,Nchange(2,:));
h=0.001;
for i = 1 : 1 : M * N do
    a1(i) = abs(P1((1000 + i) * h));
    a2(i) = abs(P1((1200 + i) * h));
    b1(i) = abs(P2((1000 + i) * h));
    b2(i) = abs(P2((1200 + i) * h));
end for
n=1;A1=A;
for i = 1 : 1 : M do
    for j = 1 : 1 : N do
        if mod(n, 2) == 0 then
            k(n) = mod (floor(a1(n) * 10^4), 256);
        else
            k(n) = mod (floor(a2(n) * 10^4), 256)
        end if
        A1(i, j) = bitxor(A(i, j), k(n));
        n=n+1;
    end for
end for
A2 (:,Nchange(2,:)) = A2 (:,Nchange(1,:));
A2 (Mchange(2,:),:) = A2 (Mchange(1,:),:);
imshow(A1);
% Decryption process:
n=1;A2=A1;
for i = 1 : 1 : M do
    for j = 1 : 1 : N do
        if mod(n, 2) == 0 then
            k1(n) = mod (floor(b1(n) * 10^4), 256);
        else
            k1(n) = mod (floor(b2(n) * 10^4), 256)
        end if
        A2(i, j) = bitxor(A1(i, j), k1(n));
        n=n+1;
    end for
end for
imshow(A2);
```

Algorithm 2 Color image encryption algorithm based on the proposed chaotic synchronization scheme.

```
A=imread('lena1.png');
[M,N]=size(A);
imshow(A);
A0=A;
% Encryption process:
Rm = randsample(M,M)';
Mchange = [1:1:M;Rm];
Rn = randsample(N,N)';
Nchange = [1:1:N;Rn];
A (Mchange(1,:),:,:) = A (Mchange(2,:),:,:);
A (:,Nchange(1,:),:) = A (:,Nchange(2,:),:);
h=0.001;
for i = 1 : 1 : M * N do
    c1(i) = abs((P1((500 + i) * h));
    c2(i) = abs(P1((1000 + i) * h));
    d1(i) = abs(P2((500 + i) * h));
    d2(i) = abs(P2((1000 + i) * h));
end for
n=1; A1=A;
for i = 1 : 1 : M do
    for j = 1 : 1 : N do
        if mod(n, 2) == 0 then
            k(n) = mod (floor(c1(n) * 10^4.5), 256);
        else
            k(n) = mod (floor(c2(n) * 10^4.5), 256)
        end if
        A1(i, j, 1) = bitxor(A(i, j, 1), k(n));
        A1(i, j, 2) = bitxor(A(i, j, 2), k(n));
        A1(i, j, 3) = bitxor(A(i, j, 3), k(n));
        n=n+1;
    end for
end for
imshow(A1);
% Decryption process:
n=1;A2=A1;
for i = 1 : 1 : M do
    for j = 1 : 1 : N do
        if mod(n, 2) == 0 then
            k1(n) = mod (floor(d1(n) * 10^4.5), 256);
        else
            k1(n) = mod (floor(d2(n) * 10^4.5), 256)
        end if
        A2(i, j, 1) = bitxor(A1(i, j, 1), k1(n));
        A2(i, j, 2) = bitxor(A1(i, j, 2), k1(n));
        A2(i, j, 3) = bitxor(A1(i, j, 3), k1(n));
        n=n+1;
    end for
end for
A2 (:,Nchange(2,:),:) = A2 (:,Nchange(1,:),:);
A2 (Mchange(2,:),:,:) = A2 (Mchange(1,:),:,:);
imshow(A2);
```

References

1. X. Chai, J. Zhang, Z. Gan, Y. Zhang, Medical image encryption algorithm based on latin square and memristive chaotic system, *Multimed Tools Appl.*, **78** (2019), 35419–35453.
2. J. He, B. Lai, A novel 4d chaotic system with multistability: Dynamical analysis, circuit implementation, control design, *Mod. Phys. Lett. B*, **33** (2019), 1950240.
3. S. Zhang, Y. Zeng, Z. Li, M. Wang, L. Xiong, Generating one to four-wing hidden attractors in a novel 4d no-equilibrium chaotic system with extreme multistability, *Chaos*, **28** (2018), 013113.
4. Q. Li, S. Liu, Switching event-triggered network synchronization for chaotic systems with different dimensions, *Neurocomputing*, **311** (2018), 32–40.
5. C. Wang, R. Chu, J. Ma, Controlling a chaotic resonator by means of dynamic track control, *Complexity*, **21** (2015), 370–378.
6. A. Mansouri, X. Wang, A novel one-dimensional sine powered chaotic map and its application in a new image encryption scheme, *Inf. Sci.*, **520** (2020), 46–62.
7. U. E. Kocamaz, S. Cicek, Y. Uyaroglu, Secure communication with chaos and electronic circuit design using passivity-based synchronization, *J. Circuit. Syst. Comp.*, **27** (2018), 1850057.
8. Q. Li, S. Liu, Y. Chen, Combination event-triggered adaptive networked synchronization communication for nonlinear uncertain fractional-order chaotic systems, *Appl. Math. Comput.*, **333** (2018), 521–535.
9. Y. Yang, L. Wang, S. Duan, L. Luo, Dynamical analysis and image encryption application of a novel memristive hyperchaotic system, *Opt. Laser Technol.*, **133** (2021), 106553.
10. Z. Yang, D. Liang, D. Ding, Y. Hu, Dynamic behavior of fractional-order memristive time-delay system and image encryption application, *Mod. Phys. Lett. B*, **35** (2021), 2150271.
11. X. Wang, Y. Su, Image encryption based on compressed sensing and dna encoding, *Signal Process-Image*, **95** (2021), 116246.
12. R. Luo, Y. Wang, Finite-time stochastic combination synchronization of three different chaotic systems and its application in secure communication, *Chaos*, **22** (2012), 023109.
13. Q. Li, S. Liu, Y. Chen, Finite-time adaptive modified function projective multi-lag generalized compound synchronization for multiple uncertain chaotic systems, *Int. J. Ap. Math. Com-pol*, **28** (2018), 613–624.
14. A. J. Munoz-Vazquez, J. D. Sanchez-Torres, C. A. Anguiano-Gijon, Single-channel predefined-time synchronisation of chaotic systems, *Asian J. Control*, **23** (2021), 190–198.
15. Y. Li, X. Yang, L. Shi, Finite-time synchronization for competitive neural networks with mixed delays and nonidentical perturbations, *Neurocomputing*, **185** (2016), 242–253.
16. X. Liu, H. Su, M. Z. Q. Chen, A switching approach to designing finite-time synchronization controllers of coupled neural networks, *IEEE T. Neur. Lear.*, **27** (2016), 471–482.
17. S. P. Bhat, D. S. Bernstein, Finite-time stability of continuous autonomous systems, *SIAM J. Control Optim.*, **38** (2000), 751–766.
18. L. Wang, T. Dong, M. Ge, Finite-time synchronization of memristor chaotic systems and its application in image encryption, *Appl. Math. Comput.*, **347** (2019), 293–305.

19. X. Cai, J. Wang, S. Zhong, K. Shi, Y. Tang, Fuzzy quantized sampled-data control for extended dissipative analysis of t-s fuzzy system and its application to wpgss-sciencedirect, *J. Franklin I.*, **358** (2021), 1350–1375.
20. L. Hua, H. Zhu, K. Shi, S. Zhong, Y. Tang, Y. Liu, Novel finite-time reliable control design for memristor-based inertial neural networks with mixed time-varying delays, *IEEE T. Circuits-I*, **68** (2018), 1599–1609.
21. G. Ji, H. Cheng, J. Yu, H. Jiang, Finite-time and fixed-time synchronization of discontinuous complex networks: A unified control framework design, *J. Franklin I.*, **355** (2018), 4665–4685.
22. X. Yang, J. Lam, D. W. C. Ho, Z. Feng, Fixed-time synchronization of complex networks with impulsive effects via non-chattering control, *IEEE T. Automat. Contr.*, **62** (2017), 5511–5521.
23. A. Polyakov, Nonlinear feedback design for fixed-time stabilization of linear control systems, *IEEE T. Automat. Contr.*, **57** (2012), 2106–2110.
24. X. Liu, D. W. C. Ho, Q. Song, J. Cao, Finite-/fixed-time robust stabilization of switched discontinuous systems with disturbances, *Nonlinear Dynam.*, **90** (2017), 2057–2068.
25. E. Jimenez-Rodriguez, J. D. Sanchez-Torres, A. G. Loukianov, On optimal predefined-time stabilization, *Int. J. Robust Nonlin.*, **27** (2017), 3620–3642.
26. J. D. Sanchez-Torres, D. Gomez-Gutierrez, E. Lopez, A. G. Loukianov, A class of predefined-time stable dynamical systems, *Int. J. Robust Nonlin.*, **35** (2018), i1–i29.
27. C. A. Anguiano-Gijon, A. J. Munoz-Vazquez, J. D. Sanchez-Torres, G. Romero-Galvan, F. Martinez-Reyes, On predefined-time synchronisation of chaotic systems, *Chaos Soliton. Fract.*, **122** (2019), 172–178.
28. J. D. Sanchez-Torres, A. J. Munoz-Vazquez, M. Defoort, R. Aldana-Lopez, D. Gomez-Gutierrez, Predefined-time integral sliding mode control of second-order systems, *Int. J. Syst. Sci.*, (2020), 1–11. doi:10.1080/00207721.2020.1815893.
29. A. J. Munoz-Vazquez, J. D. Sanchez-Torres, D. Michael, predefined-time sliding-mode control of fractionalorder systems, *Asian J. Control*, (2020). 1–9. doi:10.1002/asjc.2447.
30. A. J. Munoz-Vazquez, G. Fernandez-Anaya, J. D. Sanchez-Torres, F. Melendeza-Vazquez, Predefined-time control of distributed-order systems, *Nonlinear Dynam.*, **103** (2021), 2689–2700.
31. A. J. Munoz-Vazquez, J. D. Sanchez-Torres, M. Defoort, S. Boulaaras, Predefined-time convergence in fractional-order systems, *Chaos Soliton. Fract.*, **143** (2021), 110571–110576.

AIMS Press